AIAA JOURNAL
Vol. 31, No. 1, January 1993

Near-Field Behavior of a Tip Vortex

A. Shekarriz,* T. C. Fu,† and J. Katz‡
Johns Hopkins University, Baltimore, Maryland 21218
and
T. T. Huang§
David Taylor Model Basin, CD/NSWC, Bethesda, Maryland 20084

The near-field behavior of a tip vortex trailing behind a low aspect ratio wing, attached to an axisymmetric body, is investigated in this paper. This study was performed in a tow tank and involved the use of particle displacement velocimetry. Evolution of the tip vortex was studied by mapping its instantaneous lateral velocity at several consecutive axial locations. The axial velocity distribution was also measured. Experiments were repeated at various Reynolds numbers and incidence angles. Repeatability was also examined at the same conditions. The results indicate that roll-up is almost complete at the trailing edge and that less than 66% of the root circulation is entrained into the vortex. At $Re_c = 2.2 \times 10^5$, the results are steady, and the spatially averaged tangential velocity agrees well with the existing models. At $Re_c < 10^5$ the entire flow stucture, including the overall circulation, fluctuates from one experiment to the next. The tangential velocity profiles seem to be dominated by secondary vortices located primarily outside of the vortex core. Axial variations in the flow structure along the parallel middlebody, during the same run, are limited to the location of these secondary vortices. The vortex is observed to expand in the afterbody region, without a change in its total strength. For all but one case ($Re_c = 2.2 \times 10^5$ and $\alpha = 10$ deg), there is a substantial axial velocity deficit within the vortex core near the trailing edge of the wing. At $Re_c < 10^5$, the axial velocity deficit increases with incidence angle and decreasing Re_c.

Nomenclature

A = area bounded within contour of integration, mm^2
C_L = lift coefficient, dimensionless
c = wing chord length, mm
l = length along contour of integration, mm
Re_c = Reynolds number based on wing chord length
r = radial distance from the tip vortex center, mm
r_1 = core radius, mm
S = wing span, mm
t = wing thickness, mm
U_∞ = freestream velocity, m/s
u = axial velocity, m/s
v_θ = tangential velocity ($r = 0$ is the vortex center), m/s
x = axial (streamwise) coordinate
y = spanwise coordinate ($y = 0$ is at the wing root)
z = normal coordinate
α = angle of attack, deg
Γ = circulation, m^2/s
θ = azimuthal or tangential direction
$\overline{\ }$ = averaged quantity
$*$ = nondimensionalized parameter

Presented as Paper 91-3307 at the AIAA 9th Applied Aerodynamics Conference, Baltimore, MD, Sept. 23-26, 1991; received Jan. 13, 1992; revision received May 5, 1992; accepted for publication May 12, 1992.

*Postdoctoral Fellow, Department of Mechanical Engineering; currently, Research Scientist, Batelle, Pacific Northwest Laboratories, Richland, WA 99352. Member AIAA.

†Graduate Student, Department of Mechanical Engineering. Member AIAA.

‡Associate Professor, Department of Mechanical Engineering. Member AIAA.

§Naval Architect, Ship Hydromechanics Department. Member AIAA.

Introduction

TIP vortex studies date back to the pioneering work of Betz.[1] Through theoretical reasoning, based on conservation of circulation and vortical dispersion, he developed a wake convolution model. This model demonstrated that the circulation distribution on a lifting surface convolved into the spirals of the tip vortex asymptotically as it evolved downstream of the wing. A comprehensive review of the underlying theory is provided by Williams.[2] The question of survivability of aircraft vortices was raised over two decades ago as a flight safety issue and was pursued by the aircraft industry. This interest resulted in an avalanche of studies.[3] Most of the attention was directed toward finding the rate of change of the tangential velocity and the strength of the trailing vortices, while addressing the issues of vortex development, stability, and breakdown. Some landmark studies in this area are the flight experiments performed by McCormick et al.[4] as well as the theoretical work by Batchelor[5] and Moore and Saffman.[6] The latter recognized the significance of axial velocity on the characteristics of a tip vortex. However, the dynamics of the tip vortex during generation on a wing and in the near field behind the trailing edge have not been studied sufficiently. The near-field behavior of a tip vortex is significant in the flow behind canard wings, helicopter blades, sails of submarines, and propeller blades, where control of tip vortex cavitation is of extreme importance.

Almost all of the velocity measurements within a tip vortex have been performed by single-point techniques (hot wire, LDV, etc.). As a result of vortex meandering, these measurement techniques fail to detect the true maxima of the tangential and axial velocities in the core.[7,8] For example, according to the semi-empirical estimates presented in Ref. 7, the measurement error in the peak tangential velocity can be as much as 35%. This problem can be resolved by performing global instantaneous velocity measurement, which is the method used in the current study.

The time-averaged tangential velocity in the vicinity of its maximum value is reported to have a logarithmic profile.[9-11] This profile was first predicted by Hoffmann and Joubert, who developed a model for turbulent line vortices that in-

cluded diffusion of angular momentum.[12] However, viscous diffusion within the near field is insignificant because of the associated long time scales. The effect of turbulent diffusion would be limited to merging the discrete vortices located within the vortex sheet.[13] Thus, the tangential velocity distribution in the near field is dominated by the spanwise distribution of circulation on the wing, the wing tip geometry including surface roughness, and the velocity distribution within the wake of the wing.

Most of the studies of axial velocity distribution within a tip vortex report a deficit within its core.[14-16] However, a few cases of velocity excess at high incidence angles (above 9 deg), have also been reported.[17,18] Measurements have mostly been performed in the far field (more than 50 chord lengths downstream of the wing), where diffusive processes have expanded the vortex. Theoretical predictions of the axial velocity[5,6] are based on the assumption that the axial velocity perturbation $u-U_\infty$, and the tangential velocity v_θ, are much smaller than U_∞. Although this approximation may be acceptable in the far field, as shown by Ciffone and Orloff,[14] it is not necessarily true in the near field,[18] as will be shown in this paper.

In the current study, particle displacement velocimetry (PDV) is implemented to measure the global instantaneous velocity distribution within a tip vortex. The objective is to investigate the near-field characteristics of this vortex, including its evolution with time and dependence on incidence angle and Reynolds number.

Setup and Procedure

Figure 1a is a schematic description of the setup in the 140-ft towing tank located at the David Taylor Model Basin. The lifting surface producing the tip vortex was a low aspect ratio (0.603) uncambered rectangular wing (sail), with the dimensions and orientation as depicted in Fig. 1b. The wing is attached to a 0.3-m diam axisymmetric submarine model (DARPA SUBOFF body)[19] that has a total length of 2.61 m and includes the following sections: 0.60-m forebody, 1.34-m parallel middlebody, and 0.67-m afterbody. The leading edge of the sail is located 0.55 m from the nose of the model. The angle of attack α was set by changing the yaw angle of the model without changing the orientation of the wing relative to the body. Data were collected for six different conditions: $\alpha=5$ and 10 deg, and $Re_c=3.6\times10^4$, 7.2×10^4, and 2.2×10^5 (corresponding to freestream velocities ranging from 0.15 to 0.91 m/s). No trip wires were used on the model or on the wing.

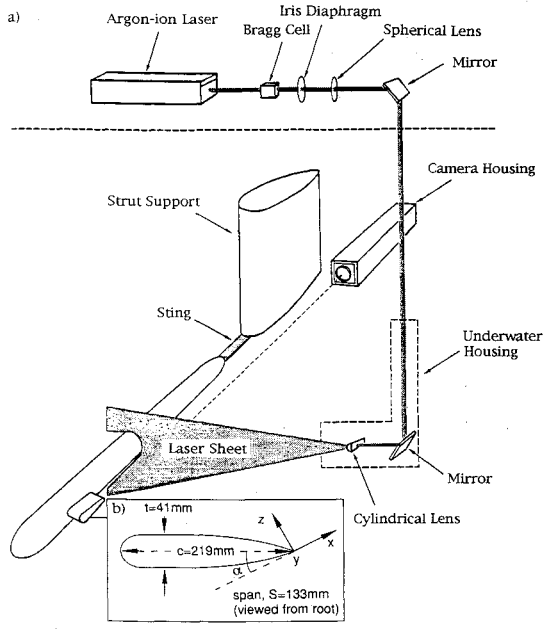

Fig. 1 Experimental setup; a) schematic description, b) wing geometry.

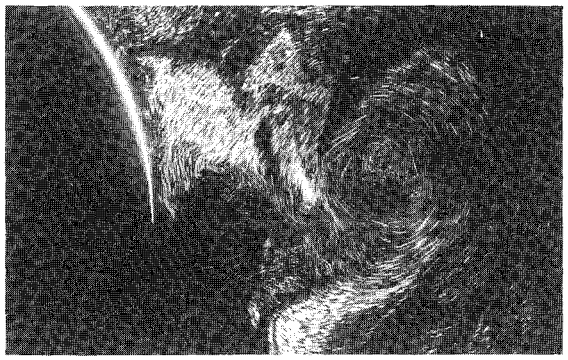

Fig. 2a Qualitative flow visualization image of the tip vortex at $x/c = 0.94$, $\alpha = 5$ deg, and $Re_c = 7.2 \times 10^4$.

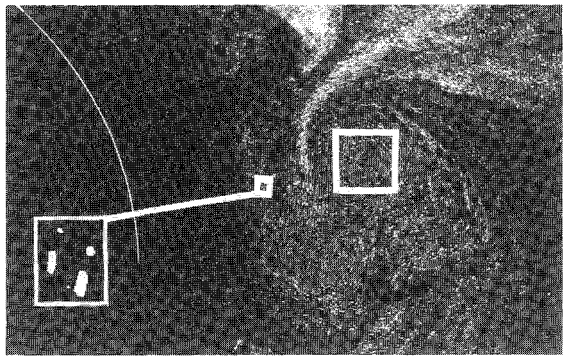

Fig. 2b Double-exposed image at $x/c = 1.97$, $\alpha = 5$ deg, and $Re_c = 7.2 \times 10^4$.

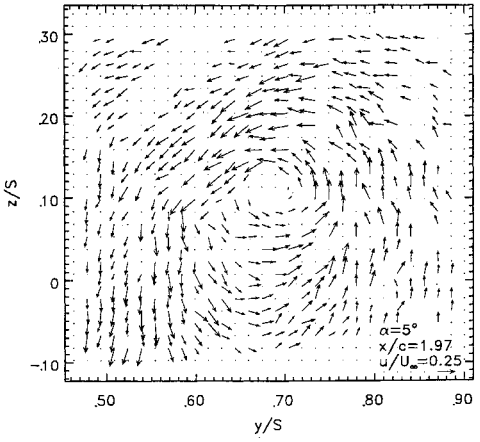

Fig. 2c Velocity vector map computed from the data enclosed within the central square in Fig. 2b.

Details on the experimental setup and procedure, including the data analysis procedures, may be found in Refs. 20 and 21. Briefly, PDV enables measurement of the instantaneous velocity distribution within a planar section of the flow. It consists of determining the displacement of a large number of microscopic (~ 25 μm in diameter), neurally buoyant (specific gravity varying between 0.95 and 1.05) tracer particles over a short time interval. The particles contain imbedded fluorescent dye (Rhodamine 6G and Dichloro-Fluorescein) and, as a result, become clearly visible while being illuminated by a green laser sheet. By pulsing this laser twice while recording a single image, each particle leaves two traces on the same film. Separate laser sheets, oriented alternately normal and parallel to the freestream, are used for determining all three components

of the velocity. The delay between pulses is on the order of 1 and 10 ms for the axial and lateral velocity measurements, respectively. Most images are recorded by a submerged 35 mm camera on Kodak TMAX-3200 film, primarily because it meets the resolution requirements[20,21] ($\sim 3500 \times 2500$ pixels for a 35 mm negative).

The negatives are then digitized by either a video or a diode array scanner. Two types of analysis procedures have been developed.[20,21] The first consists of matching traces of the same particle and measuring the distance between them (particle tracking). The direction of flow is identified by making one of the traces shorter. Calibration experiments[20] have shown that the uncertainty while using this method is below 10% (for most of the data the error is about 5%). The second procedure

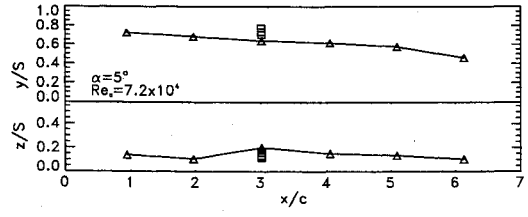

Fig. 3 Location of the tip vortex centerline.

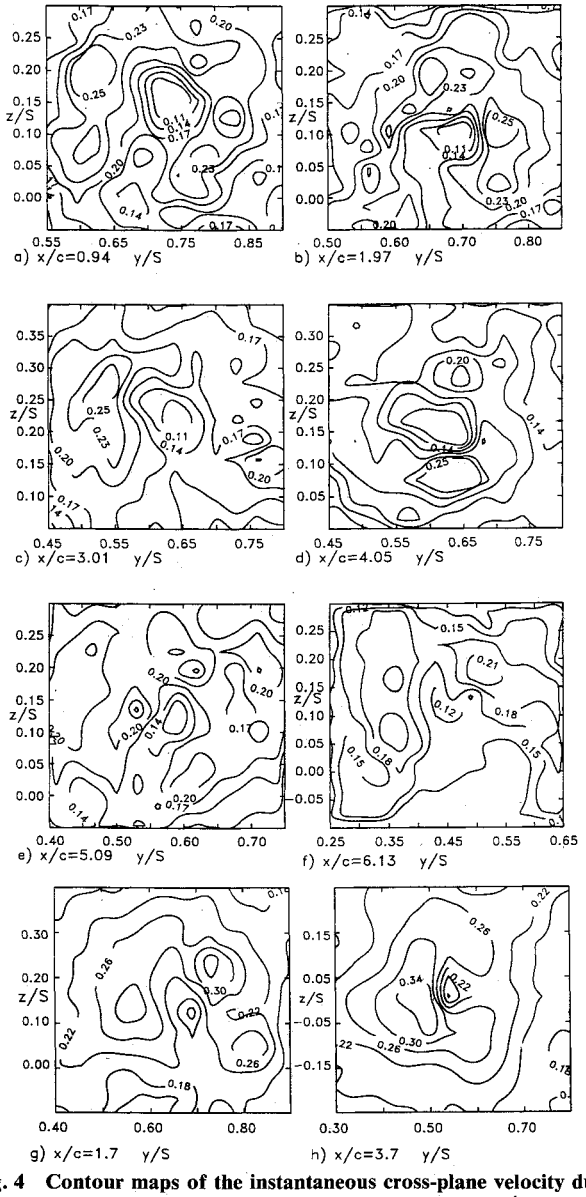

Fig. 4 Contour maps of the instantaneous cross-plane velocity during the same experiment at $\alpha = 5$ deg and $Re_c = 7.2 \times 10^4$ (a–f) and $\alpha = 10$ deg and $Re_c = 2.2 \times 10^5$ (g–h).

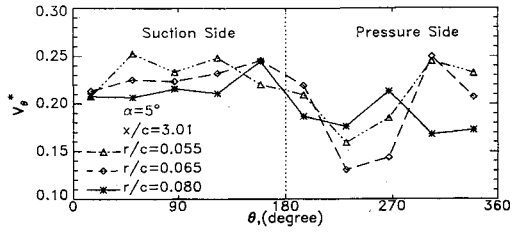

Fig. 5 Circumferential distribution of the instantaneous tangential velocity at $\alpha = 5$ deg and $Re_c = 7.2 \times 10^4$ ($v_\theta^* = v_\theta/U_\infty$).

consists of dividing the image into a large number of small sections and determining the average displacement of all particles within each section by computing the autocorrelation function of the intensity distribution (autocorrelation method). The analysis can be performed either in the spatial domain or in the frequency domain by computing the Fourier transform of the original image, either numerically [by using fast Fourier transform (FFT)] or optically (speckle velocimetry method). Calibration experiments[21] have shown that the error level can be kept at about 1%, provided several conditions, such as particle density and magnification, are satisfied. The autocorrelation technique has a directional ambiguity problem since it requires identical pulses. To resolve this problem the image of the second trace is shifted by towing the camera at the same velocity as the model. Both analysis procedures have been used in the present study. The velocity distribution in the normal plane (lateral sheet) was determined by using the particle tracking method, whereas images of the axial sheet were analyzed by using the autocorrelation method. Sample photographs of both a qualitative image containing extended particle traces and a double exposure image containing traces with different lengths, are presented in Figs. 2a and 2b, respectively. A typical vector map of the flow near the vortex core, computed from part of Fig. 2b, is presented in Fig. 2c.

Results and Discussion

Vortex Location

A series of images was recorded during each run at various axial locations starting from the trailing edge of the wing ($x/c = 0$) up to $x/c = 6.7$. Figure 3 displays the location of the tip vortex center. The solid line represents data recorded during a single run, and additional points are provided to demonstrate variations between runs. Vortex meandering is observed both at a given station (axial position) as well as from one station to the next. Variations in spanwise location y of the center are substantially higher than those in the normal direction z. In the afterbody region ($x/c > 6$), as the hull diameter starts decreasing, the vortex center also migrates inward, decreasing y.

Instantaneous Velocity

Figures 4a–4f are the instantaneous contour maps of the velocity in the crossplane at consecutive time steps; i.e., they are computed from data recorded during the same experiment. To interpret the information in these plots, note that V_θ is the dominating velocity in the vicinity of the vortex core (true for all of the data presented in Figs. 4a–4h). Consequently, the vorticity can be estimated by computing $1/r[(\partial(rV_\theta)/\partial r)$, and as long V_θ is not proportional to $1/r$ (almost nowhere in the present range), the vorticity is not zero. Within the enclosed contours located in the annular area surrounding the core, where V_θ is almost constant, the vorticity is approximately equal to V_θ/r. Such a region exits, for example, to the right of the center in Fig. 4b, and, in fact, the corresponding image and vector map (Figs. 2b and 2c) indicate the presence of secondary vortices at the same location. Traces of similar secondary structures, all of them rotating in the same direction as the tip vortex (counter clockwise), are evident in all of the

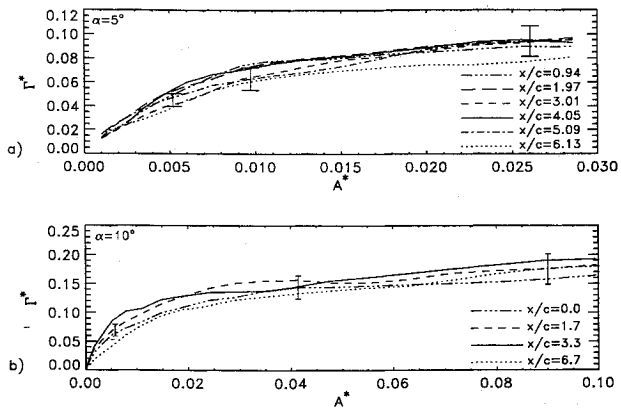

Fig. 6 Distribution of dimensionless circulation at a) $\alpha = 5$ deg and $Re_c = 7.2 \times 10^4$; b) $\alpha = 10$ deg, $Re_c = 2.2 \times 10^5$, $A^* = \pi(r/c)^2$ and $\Gamma^* = \Gamma/U_\infty c$.

contour plots presented in Fig. 4a–4e. Qualitative examination of the original photographs confirms their presence. Their origin may be the result of tip separation[22] or the vortex sheet generated behind the wing.[1–6]

When the Reynolds number and incidence angle are increased to 2.2×10^5 and 10 deg, respectively (Figs. 4g and 4h), the flow structure around the core becomes considerably more symmetric and the presence of secondary vortices is much less evident. Increased shear stresses, resulting from the higher velocity, may be the reason for their breakup. However, much denser velocity maps, recorded at smaller time intervals, are required to confirm this hypothesis (subject for future studies). Another fact, clearly evident in these figures, is the lack of symmetry in the velocity field. This phenomenon is also demonstrated in Fig. 5, where the angular distribution of the instantaneous tangential velocity is plotted. It is evident that the velocity is higher on the suction side, sometimes by as much as 40%. These variations are substantially higher than the maximum time-averaged velocity variation of 10%, measured by Higuchi et al.[11]

Circulation

The circulation of the vortex at different radial locations was computed by using the equation

$$\Gamma = \sum_i \bar{v}_i \cdot \Delta\bar{l}_i$$

where $\bar{v}_i$ and $\Delta\bar{l}_i$ are the velocity and length of each segment along the contour, respectively. Concentric circular contours, adjusted to the center of the vortex (within $0.01c$), were used. Linear interpolation was used in regions with missing vectors, and the interpolation error was evaluated by comparing known vectors with estimated values. The uncertainty in the circulation ranged between 12–18%, including both the measurement and interpolation errors. Figures 6a and 6b are profiles of circulation computed from the instantaneous velocity distributions shown in Figs. 4a–4h. The slope of each line is a measure of the local mean vorticity, since the abscissa is the dimensionless area enclosed by the contour of integration, $A^* = \pi(r/c)^2$. As expected, the vorticity is highest at the center of the vortex, and it approaches zero outside of the core. Since a vortex sheet is entrained from the pressure side, the vorticity does not completely vanish with increasing A^*. In computing the circulation profile, integration was terminated when the vorticity became less than 10% of that at the center. Note that the circulation profiles for $x/c < 6$ vary by about 25% at the intermediate range of A^* ($0.005 < A^* < 0.015$ in Fig. 6a and $0.005 < A^* < 0.03$ in Fig. 6b). These variations can be linked to the presence of the secondary vortices that surround the vortex core as discussed earlier in conjunction with Fig. 4. The sudden change in circulation observed at $x/c > 6$, in both Figs. 6a and 6b, results from narrowing of the body. Both axial and lateral pressure gradients, produced by the model, expand the tip vortex. Note that the overall circulation recovers to its previous values at a larger radius in Fig. 6b.

According to the data obtained by Roddy,[19] on the same body-wing geometry and at $Re_c \sim 10^6$, the lift coefficient ($\bar{C}_L$) is 0.3 and 0.57 for incidence angles of 5 and 10 deg, respectively. Thus, the resulting $\bar{C}_L/\alpha$, where α is in radians, are 3.44 and 3.26, respectively—nearly half of the theoretical value for a flat plate. The dimensionless mean circulations, estimated from $\Gamma/(U_\infty c) = 0.5\bar{C}_L$, are, in turn, 0.15 and 0.29. Thus, the results presented in Fig. 6 show that only 66% of the mean circulation is rolled-up into the tip vortex. Since the root circulation is higher than $\bar{\Gamma}$, the rolled-up portion of the root circulation is even less than 66%. Results of previous experimental studies range between a minimum of 45%[4,11] to a maximum of 80%.[9] Thus, the tip vortex circulation, determined from the instantaneous velocity distribution, is still much lower than the wing circulation, as estimated from the lift coefficient.

The convective velocities of the vortex sheet, when estimated from $\bar{u}_c = \bar{\Gamma}/2S$[23] suggest that roll-up should continue up to $x/c \sim 5$ and ~ 2.5 for the cases described in Figs. 6a and 6b, respectively. It is obvious that the results presented in these figures do not agree with these predictions, since at $x/c = 0$ the vortex has already reached 85% of its maximum measured strength (Fig. 6b). Further downstream, the overall circulation remains constant within the measurement error. These observations are consistent with previous studies reporting that roll-up of the tip vortex begins at the leading edge of the wing.[22–24] Therefore, the classical models that consist only of roll-up of the vortex sheet are incomplete and require modifications to incorporate generation of the tip vortex on the wing.

Dependence on Reynolds number and angle of incidence were examined at $Re_c = 3.6 \times 10^4$, 7.2×10^4, and 2.2×10^5 for $\alpha = 5$ and 10 deg. Results, containing averaged profiles computed from at least three instantaneous velocity distributions, are presented in Figs. 7a and 7b. Figure 7a shows that the slope of the circulation curves increases with Reynolds number within the core of the vortex ($A^* < 0.005$). Outside of the core, the increase is significantly slower and more uniform at

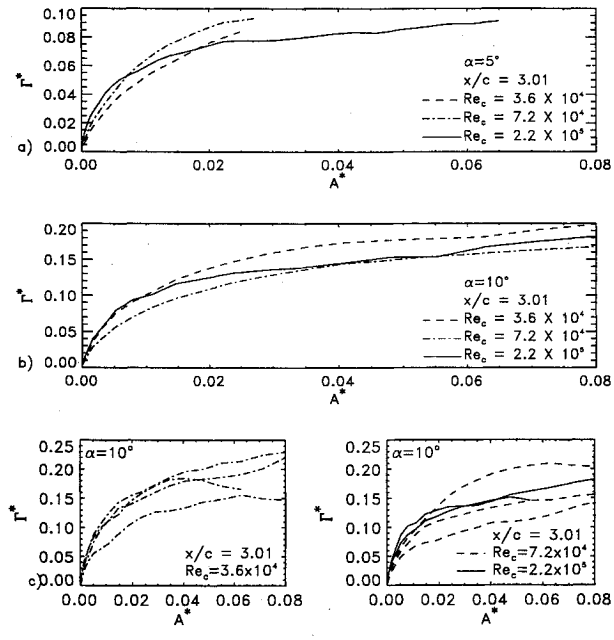

Fig. 7 Mean circulation distribution at different Reynolds numbers for a) $\alpha = 5$ deg, b) $\alpha = 10$ deg, and c) several instantaneous distributions used for computing the mean values presented in Figs. 7a and 7b.

Re_c, $= 2.2 \times 10^5$. Higher levels of turbulence and mixing may be an explanation for this trend. As noted before, at this Re_c the tip vortex also contains fewer secondary structures, probably due to higher levels of shear. When the incidence angle is increased to 10 deg (Fig. 7b), the core vorticity does not show the same trend with increasing Reynolds numbers. By examining all of the available data at $x/c \sim 3$, it was determined that the apparent inconsistency was a result of fluctuations in the circulation profile and overall strength of the vortex. These fluctuations tend to increase with the incidence angle and, as a result, are more significant at 10 than at 5 deg, and decrease with the Reynolds number. As illustrated by the instantaneous distribution presented in Fig. 7c, the results are fairly steady at $Re_c = 2.2 \times 10^5$, whereas at $Re_c = 3.6 \times 10^4$ the vortex strength fluctuates by as much as 50% at both incidence angles (only data at 10 deg is shown). In an attempt to find an explanation for this phenomenon, the cross-plane images of the flow near the surface of the wing were examined qualitatively. They show that at $Re_c = 2.2 \times 10^5$ the boundary layer is already turbulent (containing a large number of small, evenly distributed vortices), whereas at the lower Reynolds numbers the flow near the surface appears to be unsteady and transitional (characterized by intermittent appearance of vortices). Thus, the high level of fluctuations at $Re_c < 10^5$ are believed to be linked to boundary-layer transition on the surface of the wing.

Tangential Velocity

Distributions of the normalized average tangential velocity, $\bar{v}_\theta^* = \Gamma/(2\pi r U_\infty)$, computed from the instantaneous data (Fig. 5), are presented in Figs. 8a and 8b. Because of a limited number of available data points, the distribution at $x/c = 0$ (Fig. 8b) is not extended into the core. However, a few instantaneous vectors have peak values of about 45% of U_∞ at $r/c \sim 0.04$. As expected, the peak average tangential velocity $\bar{v}_{\theta,\max}^*$ increases with the incidence angle from 22% at 5 deg to 34% at 10 deg. The ratio of these maximum velocities (1.55) is smaller than the corresponding ratio of lift coefficients (1.9, according to Ref. 19), unlike results presented in Ref. 4, where it is concluded that the normalized velocity is proportional to the lift coefficient. However, the overall strength of the tip vortex at the same Re_c is proportional to α (see Fig. 7a). Note also that the values of $\bar{v}_{\theta,\max}^*$ vary by as much as 20% from section to section, primarily due to entrainment of and migration of secondary structures, as well as core expansion resulting from narrowing of the body at $x/c > 6$.

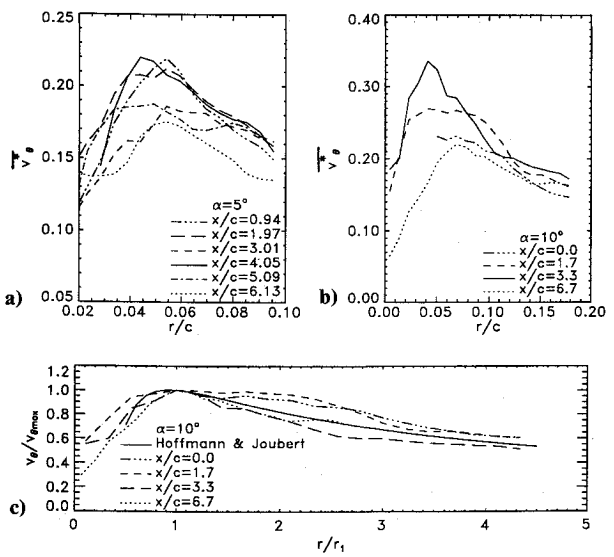

Fig. 8 Circumferentially averaged tangential velocity, $\bar{v}_\theta^* = \Gamma/(2\pi r U_\infty)$, at a) $\alpha = 5$ deg, $Re_c = 7.2 \times 10^4$; b) $\alpha = 10$ deg, $Re_c = 2.2 \times 10^5$; and c) normalized tangential velocity distribution at $Re_c = 2.2 \times 10^5$.

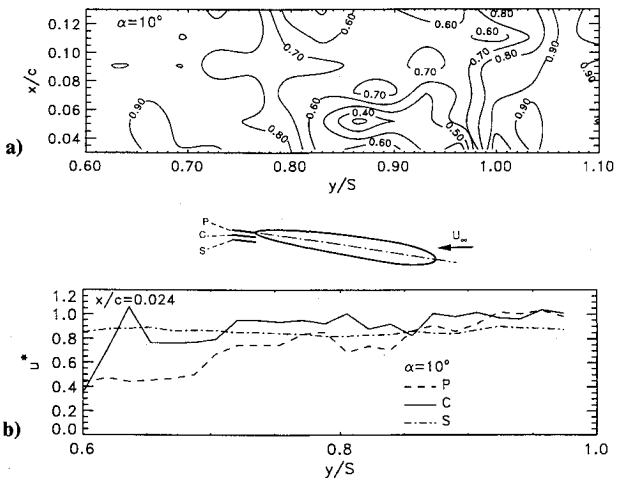

Fig. 9 Axial velocity: a) contour map of the dimensionless axial velocity ($u^* = u/U_\infty$) within and in the vicinity of a tip vortex at $\alpha = 10$ deg and $Re_c = 7.4 \times 10^4$; and b) dependence of axial velocity on z, $\alpha = 10$ deg and $Re_c = 2.2 \times 10^5$.

The core size r_1/c, defined as the radius at which $\bar{v}_\theta^*$ is a maximum, is 0.05 and 0.04 at 5- and 10-deg incidence, respectively. According to Moore and Saffman,[6] r_1/c is equal to $2.92(x/c)^{0.5} Re_c^{-0.5}$ for an elliptically loaded wing. Although the currently observed trend with Re_c agrees with their conclusions qualitatively, the 20% decrease in radius is much smaller than the 58% decrease predicted by their equation (based on a ratio of 3:1 in Re_c). Furthermore, the axial changes in r_1/c are quite small and are definitely not proportional to $(x/c)^{0.5}$. In fact, the only noticeable change in core size occurs due to narrowing of the body.

It is also interesting to compare the present results with the vorticity diffusion model developed by Hoffmann and Joubert.[12] This task is quite difficult in a flow dominated by secondary vortices (such as the present low Re_c data), since it requires an accurate measure of the core size. When the location of $\bar{v}_{\theta,\max}^*$ can be determined reliably, as in Fig. 8b, then the normalized tangential velocity distributions agree with Hoffmann and Joubert's results (Fig. 8c). This conclusion is also consistent with the experimental results of Ref. 11.

Axial Velocity

The two primary mechanisms that affect the axial velocity in the core of a tip vortex are[5,6] 1) momentum deficit caused by the boundary layer on the wing and 2) axial variation of the core tangential velocity. The latter gives rise to an axial pressure gradient and in turn to a change in the axial velocity. For example, radial diffusion of the tangential momentum results in an increase in the core pressure and a reduction in the axial velocity. This phenomenon is typically observed within a vortex that is decaying,[14-16] expanding,[17] or subjected to breakdown.[3] Conversely, during vortex roll-up,[9] the tangential velocity increases with x/c, creating a negative axial pressure gradient and, consequently, an increase in the axial velocity. Thus, the boundary layer on the wing and vortex roll-up have opposite effects. Since the axial pressure gradient also depends on r, one may find that in some portion of a tip vortex there is axial momentum deficit, whereas in another a momentum excess.[17,18]

In the present study, the axial velocity within the tip vortex was measured within an x-y plane, located at $z \simeq 0$, and extending from the trailing edge of the wing ($x \geq 0$). Figure 9a is a typical contour map of u^*, the instantaneous axial velocity scaled with U_∞. Note that, at the inboard side of the vortex ($y/S < 0.8$), the visualized plane is located within the wake of the wing, and as a result u^* is only about 0.88. Within the spanwise range $0.82 < y/S < 0.98$, namely in the vicinity of the vortex core (determined from the lateral sheets), the velocity

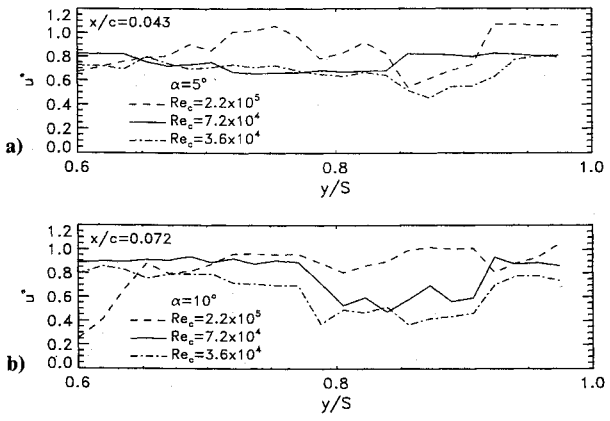

Fig. 10 Dependence of axial velocity on Reynolds number at a) $\alpha = 5$ deg and b) $\alpha = 10$ deg.

deficit is even larger ($u^* < 0.65$). The size of this range is almost the same as the diameter of the vortex core presented in Fig. 8. Further outboard, the axial velocity quickly recovers to the freestream conditions ($u^* \dashrightarrow > 1$).

To investigate variations in the z-direction, the axial flow was visualized in three planes, located at $z/S = 0$, 0.09, and 0.18. Typical spanwise velocity distributions at the trailing edge of the wing are presented in Fig. 9b. For convenience, the plane crossing the vortex center is marked as C; the planes located close to the pressure and suction sides of the wing are marked as P and S, respectively. The vortex-induced velocity deficits in all three planes are considerably smaller than the results in Fig. 9a (note the Re_c difference) and extend over a smaller region ($0.8 < y/S < 0.87$). Consistent with its location relative to the surface (boundary layer) of the wing, the axial velocity in the P section is considerably lower for most of the wing span. The velocity in the S section remains almost constant and unaffected by the presence of the vortex.

Dependence of the axial velocity on Re_c, and α is demonstrated in Fig. 10. These profiles, although instantaneous, show typical behavior for each test condition. Besides one case ($Re_c = 2.2 \times 10^5$ and $\alpha = 10$ deg), the axial velocity in the vicinity of the vortex core is considerably lower than U_∞. For $Re_c < 10^5$, the deficit in velocity appears to increase with increasing α and decreasing Re_c. These results are consistent with the observations in the lateral planes. Since the maximum (average or instantaneous) tangential velocity and core radius do not change significantly with x/c (Figs. 4a–4f and Fig. 8a), the axial pressure gradients are small. Thus, the only mechanism affecting the axial velocity is the momentum deficit within the boundary layer. For a laminar flow, one would expect a larger deficit when the boundary layer is thicker, namely at a lower Re_c or a higher incidence angle.

Conclusions

The near-field behavior of a tip vortex trailing behind a low aspect ratio rectangular wing attached to an axisymmetric body is investigated by implementing PDV. The results lead to the following conclusions:

1) Roll-up of the tip vortex is complete almost immediately downstream of the trailing edge of the wing ($x/c < 1$). The overall circulation of this vortex remains nearly constant throughout the range of x/c studied ($0 < x/c < 6.7$).

2) Less than 66% of the root circulation is rolled up into the tip vortex, even when the circulation is computed from the instantaneous velocity distribution.

3) Expansion of the tip vortex (an increase in the radius of the core and a reduction in the tangential velocity) occurs as a result of adverse axial pressure gradients caused by contraction of the body at $x/c > 6$.

4) The circulation and tangential velocity profiles in the near field are dominated by the presence of the secondary vortices. As the Reynolds number is increased beyond 10^5, their impact diminishes, and the velocity profile begins to resemble the classical results of Hoffmann and Joubert.[12]

5) The velocity distribution and the overall circulation of the tip vortex become increasingly unsteady as the Reynolds number is reduced and the incidence angle is increased. Boundary-layer transition on the wing is suspected to be the primary reason.

6) When averaged over several runs, the overall circulation of the tip vortex scales with the Re_c and the incidence angle.

7) For the present test conditions, the axial velocity in the near field is dominated by the boundary layer on the wing. Consequently, for all but one case ($Re_c = 2.2 \times 10^5$ and $\alpha = 10$ deg), there is substantial velocity deficit within the tip vortex core.

Acknowledgments

This work was supported by the Independent Research and Independent Exploratory Development Program of the David Taylor Model Basin and the Submarine Technology Program of the Defense Advanced Research Projects Agency. We are grateful to Gary Jones of DARPA for his continued support.

References

[1]Betz, A., "Verhalten von Wirbelsystemen," *Z. agnew. Math. Mech.*, Vol. 12, No. 164, 1932; also NACA TM 713.

[2]Williams, G. M., "Viscous Modelling of Wing-Generated Trailing Vortices," *Aeronautical Quarterly*, Vol. 25, May 1974, pp. 143–154.

[3]Olsen, H. A., Goldberg, A., and Rogers, M. (eds), "Aircraft Wake Turbulence and its Detection," Plenum Press, 1971.

[4]McCormick, B. W., Tangler, J. L., and Sherrieb, H. E., "Structure of Trailing Vortices," *Journal of Aircraft*, Vol. 5, No. 3, 1968, pp. 260–267.

[5]Batchelor, G. K., "Axial Flow in Trailing Line Vortices," *Journal of Fluid Mechanics*, Vol. 20, Pt. 4, 1964, pp. 645–658.

[6]Moore, D. W., and Saffman, P. G., "Axial Flow in Laminar Trailing Vortices," *Proceedings of the Royal Society of London*, Series A, Vol. 333, 1973, pp. 491–508.

[7]Baker, G. R., Barker, S. J., Bofah, K. K., and Saffman, P. G., "Laser Anemometer Measurements of Trailing Vortices in Water," *Journal of Fluid Mechanics*, Vol. 65, Pt. 2, 1974, pp. 325–336.

[8]Corsiglia, V. R., Schwind, R. G., and Chigier, N. A., "Rapid Scanning, Three-Dimensional Hot-Wire Anemometer Surveys of Wing-Tip Vortices," *Journal of Aircraft*, Vol. 10, No. 12, 1973, pp.752–757.

[9]El-Ramly, Z., and Rainbird, W. J., "Flow Survey of the Vortex Wake Behind Wings," *Journal of Aircraft*, Vol. 14, No. 11, 1977, pp. 1102–1108.

[10]Govindaraju, S. P., and Saffman, P. G., "Flow in a Turbulent Trailing Vortex," *The Physics of Fluids*, Vol. 14, No. 10, 1971, pp. 2074–2080.

[11]Higuchi, H., Quadrelli, J. C., and Farell, C., "Vortex Roll-Up from an Elliptic Wing at Moderately Low Reynolds Numbers," *AIAA Journal*, Vol. 25, No. 12, 1987, pp. 1537–1542.

[12]Hoffmann, E. R., and Joubert, P. N., "Turbulent Line Vortices," *Journal of Fluid Mechanics*, Vol. 16, 1963, pp. 395–411.

[13]Phillips, W. R. C., "The Turbulent Trailing Vortex During Roll-up," *Journal of Fluid Mechanics*, Vol. 105, 1981, pp. 451–467.

[14]Ciffone, D. L., and Orloff, K. L., "Axial Flow Measurements in Trailing Vortices," *AIAA Journal*, Vol. 12, No. 2, Aug. 1974, pp. 1154–1155.

[15]Logan, A. H., "Vortex Velocity Distributions at Large Downstream Distances," *AIAA Journal*, Vol. 8, No. 11, 1970, pp. 930–932.

[16]Olson, J. H., "Results of Trailing Vortex Studies in a Towing Tank," *Aircraft Wake and Its Detection*, edited by J. H. Olsen, A. Goldburg, and M. Rogers, Plenum Press, New York, 1971, pp. 455–472.

[17]Chigier, N. A., and Corsiglia, V. R., "Wind-Tunnel Studies of Wing Wake Turbulence," *Journal of Aircraft*, Vol. 9, No. 12, 1972, pp. 820–825.

[18]Green, S. I., and Acosta, A. J., "Unsteady Flow in Trailing Vortices," *Journal of Fluid Mechanics*, Vol. 227, 1991, pp. 107–134.

[19]Roddy, R. F., "Investigation of the Stability and Control Characteristics of Several Configurations of the DARPA SUBOFF Model (DTRC Model 5470) from Captive-Model Experiments," David Taylor Research Center, DTRC-SHD-1298-08, Bethesda, MD, Sept. 1990.

[20]Shekarriz, A., Fu, T. C., Katz, J., Liu, H. L., and Huang, T. T., "Study of Junction and Tip Vortices Using Particle Displacement Velocimetry," *AIAA Journal,* Vol. 30, No. 1, 1992, pp. 145–152.

[21]Dong, R., Chu, S., and Katz, J., "Quantitative Visualization of the Flow Within the Volute of a Centrifugal Pump, Part A: Technique," *Journal of Fluids Engineering,* Vol. 114, No. 3, 1992, pp. 390–395.

[22]Katz, J., and Bueno Galdo, J., "Effect of Roughness on Rollup of Tip Vortices on a Rectangular Hydrofoil," *Journal of Aircraft,* Vol. 26, No. 3, 1989, pp. 247–253.

[23]Moore, D. W., "A Numerical Study of the Roll-up of a Finite Vortex Sheet," *Journal of Fluid Mechanics,* Vol. 63, Pt. 2, 1974, pp. 225–235.

[24]Francis, M. S., and Kennedy, D. A., "Formation of a Trailing Vortex," *Journal of Aircraft,* Vol. 16, No. 3, 1979, pp. 148–154.